Hindawi
Shock and Vibration
Volume 2019, Article ID 1915708, 12 pages
https://doi.org/10.1155/2019/1915708

Research Article

Dynamic Modeling and Parameters Optimization of Large Vibrating Screen with Full Degree of Freedom

Xiaodong Yang,[1] Jida Wu,[1] Haishen Jiang,[2] Wenqiang Qiu,[1] and Chusheng Liu[1]

[1]*School of Mechatronic Engineering, China University of Mining and Technology, Xuzhou 221116, China*
[2]*School of Chemical Engineering, China University of Mining and Technology, Xuzhou 221116, China*

Correspondence should be addressed to Jida Wu; wujidacumt@126.com

Received 21 October 2018; Revised 19 December 2018; Accepted 1 January 2019; Published 31 January 2019

Academic Editor: Davood Younesian

Dynamic characteristic and reliability of the vibrating screen are important indicators of large vibrating screen. Considering the influence of coupling motion of each degree of freedom, the dynamic model with six degrees of freedom (6 DOFs) of the vibrating screen is established based on the Lagrange method, and modal parameters (natural frequencies and modes of vibration) of the rigid body are obtained. The finite element modal analysis and harmonic response analysis are carried out to analyze the elastic deformation of the structure. By using the parametric modeling method, beam position is defined as a variable, and an orthogonal experiment on design is performed. The BP neural network is used to model the relationship between beam position and maximal elastic deformation of the lateral plate. Further, the genetic algorithm is used to optimize the established neural network model, and the optimal design parameters are obtained.

1. Introduction

The vibrating screen is one of the key equipment for coal processing, which is widely used in grading, desliming, sculpting, and dewatering of coal [1, 2]. Due to the development trend of large scale and intensification of the coal dressing plant, a large vibrating screen is urgently needed to simplify the production system and to reduce plant volume, construction investment, and operation cost. At the same time, the demand on performances and reliability of a large vibrating screen becomes higher. It has a very important significance to improve the theoretical research and level of the design of the large vibrating screen. Baragetti and Villa proposed a study of the dynamics of a heavy loaded vibrating screen based on a 3-DOF dynamic model and optimized the design parameters in order to minimize the pitching angle of the screen [3]. Wang et al. presented an optimization of the linear vibrating screen based on MATLAB Optimization Toolbox, which leads to the optimal productivity per unit power increase 28.5% in comparison with the initial value [4]. Li et al. [5] established the nonparametric model mapping the vibrating screen efficiency and operating parameters using the discrete element method and support vector machines and optimized the parameters with particle swarm optimization. He and Liu proposed a theoretical model for the dynamic behavior evaluation of vibrating screens and presented a new screen with elliptical trace [6]. Based on the experiments, Zhang established a least square support vector machine model to predict the sieving efficiency and optimize the parameters using the adaptive genetic algorithm and cross-validation algorithm [7]. As the vibrating screen belongs to the group of vibration and utilization machines, the structure is subjected to a large dynamic load, which can easily cause local elastic deformation and lead to fatigue failure in the structure. To improve the reliability of large vibrating screens, Zhao et al. presented a new design of a hyperstatic net-beam structure and analyzed dynamic characteristic of it, based on the finite element method, and the new screen proves to have much higher structural strength with an enhanced dynamic behavior [8]. Su et al. proposed an improved scheme of beam section for large-scale vibrating screen structure based on static analysis and dynamic analysis, which ameliorated stress distribution of the vibrating screen is in working

process, and the fatigue life is increased [9]. Baragetti presented a structural solution for high loaded vibrating screens with new modified side walls and studied the behavior of the original and modified structure by means of theoretical and numerical models [10]. Peng et al. conducted a systematic mechanics analysis of the beam structures and improved the design method considering bending and random vibration [11]. Wang et al. presented a novel large vibrating screen with a duplex statically indeterminate mesh beam structure. Through the model analysis result comparisons with the traditional vibrating screen, the superiority of this structure was verified [12]. Jiang et al. established a dynamic model and stability equations of the variable linear vibration screen and investigated the motion behavior of screen face as well as confirmed best range of exciting position [13]. Du et al. proposed a single-deck equal-thickness vibrating screen driven externally by an unbalanced two-axle excitation with a large span and presented 3-degree-freedom dynamic equations [14]. However, the traditional two-degree-of-freedom or three-degree-of-freedom dynamic model can only reflect the motion in plane but cannot reflect the complex motion in space. The traditional optimization method requires iterative solution and is not suitable for multivariable nonlinear model optimization, which has high computational cost and is not suitable for multivariable nonlinear model optimization.

At present, ANNs have become a preferred alternative way to solve any of complex, highly coupled, and nonlinear problems. Rad et al. constructed an expert system used Bayesian regulation back-propagation neural network and vibration monitoring data for electric motor status diagnosis [15]. Tian developed a Levenberg–Marquardt artificial neural network-based method for achieving accurate remaining useful life prediction of equipment subject to condition monitoring [16]. Meruane and Mahu trained the neural network using a noise-injection learning algorithm to reduce the effects of experimental noise [17]. Sun and Han proposed a UAV aerial photography monitoring method based on gradient descent with the momentum neural network, which improved the efficiency of automatic extraction and classification of image features [18]. Taking training time, iteration times, and error performance as indicators, Zhang et al. compared the training efficiency of BFGS quasi-Newton algorithm, resilient algorithm, LM algorithm, and Fletcher–Reeves update algorithm for the neural network model in the classification process of OCT images [19].

The article is structured as follows. In Section 2, the dynamic model with six degrees of freedom (6 DOFs) of the vibrating screen based on the Lagrange method was established, and multinatural frequency and natural modes of vibration of the vibrating screen were calculated based on rigid body modal analysis. In Section 3, the finite element method was used to analyze dynamic performance of the large vibrating screen. In Section 4, the BP neural network was used to establish the nonlinear mapping between position parameters of stiffening beams and dynamic performance of vibrating screen, and the sensitivity analysis was carried out bases on the model. The optimal combination of structural parameters was obtained using the genetic algorithm. Finally, the conclusion is drawn in Section 5.

2. Rigid Body Dynamics Analysis

2.1. The Structure of Vibrating Screen. ZS2560 is a linear vibrating screen widely used in coal separation. As shown in Figure 1, the ZS2560 linear vibrating screen is mainly composed of vibration exciters, screen box, and spring. The screen box is the main working part of the vibrating screen, and accordingly, it is vulnerable to the damage. The screen box includes both left and right sides of the plate, the tailgate, spring support group, and sill and stiffening beams. In order to adapt to heavy load conditions, the screen box of ZS2560 adopts the double-bottom beam structure instead of the traditional single-layer beam structure, which can achieve higher structural stiffness and lower center of mass. The vibration exciters are set up on the left and right sides of the plate, which can generate sinusoidal excitation force along the normal direction using two eccentric block synchronous reverse rotations. Under the action of excitation force, the entire screen box is vibrated and a sieving of the material is realized when in operation.

2.2. Rigid Body Dynamics Modeling. At present, the simplified 2-degree or 3-degree freedom mass-spring vibration model is often used in dynamic analysis of the vibrating screen [20, 21]. However, the 2-degree vibration model can only represent the linear motion of the vibrating screen in two directions, and the 3-degree freedom vibration model can represent the swing around a certain axis in addition, and it is difficult to fully reflect the complex motion of the vibrating screen. Considering the translation and rotation around the center of mass in x-y, x-z, and y-z planes at the same time, this paper establishes a 6-degree freedom vibration model of the vibrating screen (Figure 2), wherein the screen box is equivalent to the rigid body in space motion.

As shown in Figure 2, the origin of the x-O-y coordinate system is located at static equilibrium position of the screen box (the center of mass), m is the mass of the vibrating screen when it is in operation, J_x, J_y, and J_z are the moments of inertia of the center of mass of the vibrating screen with respect to x, y, and z axes, respectively, and K_x, K_y, and K_z are the stiffness of springs at front and rear positions, respectively. The distance from each spring to the center of mass is l_{ij}, where i represents the spring force direction and j represents the spacing direction. Besides, the displacements on each degree of freedom are labeled as x, y, and z, and the angles are labeled as ψ_x, ψ_y, and ψ_z. According to the mechanical model, the following equations can be obtained:

Kinetic energy of the system can be expressed as

$$T = \frac{1}{2}m\left(\dot{x}^2 + \dot{y}^2 + \dot{z}^2\right) + \frac{1}{2}\left(J_{xx}\dot{\varphi}_x^2 + J_{yy}\dot{\varphi}_y^2 + J_{zz}\dot{\varphi}_z^2\right) + J_{xy}\dot{\varphi}_x\dot{\varphi}_y + J_{xz}\dot{\varphi}_x\dot{\varphi}_z + J_{yz}\dot{\varphi}_y\dot{\varphi}_z. \quad (1)$$

Potential energy of the system can be expressed as

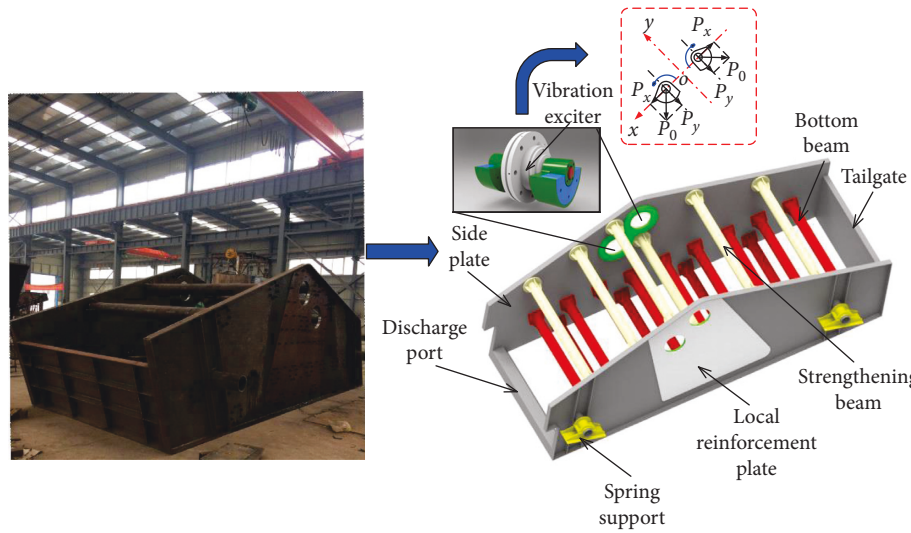

Figure 1: Schematic diagram of the ZS2560 linear vibrating screen.

$$U = \frac{1}{2}\left[\sum k_x\left(x + \varphi_y l_{xz} - \varphi_z l_{xy}\right)^2 + \sum k_y\left(y - \varphi_x l_{yz} + \varphi_z l_{yx}\right)^2 + \sum k_z\left(z + \varphi_x l_{zy} - \varphi_y l_{zx}\right)^2\right]. \tag{2}$$

The Lagrange equation with 6 degrees of freedom is shown as follows:

$$\frac{d}{dt}\left(\frac{\partial T}{\partial \dot{q}}\right) - \frac{\partial T}{\partial q} + \frac{\partial U}{\partial q} = F, \tag{3}$$

where q is the generalized coordinates matrix of the vibration system, $q = [x, y, z, \varphi_x, \varphi_y, \varphi_z]^T$; $\dot{q}$ and $\ddot{q}$ are the generalized velocities matrix and generalized acceleration matrix of the system, respectively; F is the excitation matrix of the system, $F = [f_x, f_y, f_z, M_x, M_y, M_z]^T$.

Substituting Equations (1) and (2) into Equation (3), the content of each element in the mass matrix and the stiffness matrix is calculated according to the following formula:

$$\begin{cases} m_{kl} = m_{lk} = \dfrac{\partial^2 T}{\partial \dot{q}_k \partial \dot{q}_l}, \\ k_{kl} = k_{lk} = \dfrac{\partial^2 U}{\partial q_k \partial q_l}. \end{cases} \tag{4}$$

Accordingly, the mass matrix and stiffness matrix of the system are constructed as follows:

$$M = \begin{bmatrix} m & 0 & 0 & 0 & 0 & 0 \\ 0 & m & 0 & 0 & 0 & 0 \\ 0 & 0 & m & 0 & 0 & 0 \\ 0 & 0 & 0 & J_{xx} & 0 & 0 \\ 0 & 0 & 0 & 0 & J_{yy} & 0 \\ 0 & 0 & 0 & 0 & 0 & J_{zz} \end{bmatrix},$$

$$K = \begin{bmatrix} \sum k_x & 0 & 0 & 0 & \sum k_x l_{xz} & -\sum k_x l_{xy} \\ 0 & \sum k_y & 0 & \sum k_y l_{yz} & 0 & \sum k_y l_{yx} \\ 0 & 0 & \sum k_z & \sum k_y l_{zy} & -\sum k_z l_{zx} & 0 \\ 0 & \sum k_y l_{yz} & \sum k_z l_{zy} & \sum k_y l_{yz}^2 + \sum k_z l_{zy}^2 & -\sum k_z l_{zx} l_{zy} & -\sum k_y l_{yz} l_{zx} \\ \sum k_x l_{xz} & 0 & -\sum k_z l_{zx} & -\sum k_z l_{zx} l_{zy} & \sum k_x l_{xz}^2 + \sum k_z l_{zx}^2 & -\sum k_x l_{xz} l_{xy} \\ -\sum k_x l_{xy} & -\sum k_y l_{yx} & 0 & -\sum k_y l_{yz} l_{zx} & -\sum k_x l_{xz} l_{xy} & \sum k_y l_{yx}^2 + \sum k_x l_{xy}^2 \end{bmatrix}. \tag{5}$$

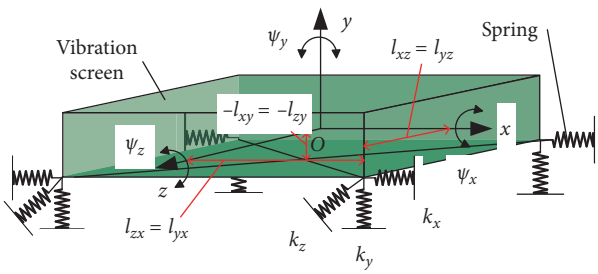

Figure 2: Sketch map of 6 degrees of freedom vibration model.

The vibration equation of the linear vibration screen is established based on the Lagrange method and it is shown that

$$\mathbf{M}\ddot{\mathbf{q}} + \mathbf{K}\mathbf{q} = \mathbf{F}, \tag{6}$$

where $\mathbf{F} = [\, \mathbf{m_0 e}\omega^2 \cos\alpha \;\; \mathbf{m_0 e}\omega^2 \sin\alpha \;\; 0 \;\; 0 \;\; 0 \;\; \mathbf{m_0 e}\omega^2\delta \,]^T$, and $\mathbf{m_0 e}$ is the product of the eccentric mass diameter of the exciter, kg m; ω is the rotation speed, rad/s; α is the vibrating direction angle, rad; δ is the normal distance between the center of mass and the excitation force direction, m.

2.3. Rigid Body Modal Analysis. Modal analysis is a common method for studying dynamic characteristics of mechanical structures and design optimization. Modal analysis of the vibrating screen can be used to obtain modal parameters, such as natural frequency and natural vibration mode, as well as to provide a reference for the revision and structure design optimization of the subsequent simulation calculation model [22, 23].

Assuming that the excitation force is equal to zero, the free vibration equation of vibrating screen is defined by the following equation:

$$\mathbf{M}\ddot{\mathbf{q}} + \mathbf{K}\mathbf{q} = \mathbf{O}. \tag{7}$$

According to the vibration theory, we can assume that the solution of Equation (7) is as follows:

$$q = \mathbf{A}e^{i\lambda t}, \tag{8}$$

where $\mathbf{A}$ is the amplitude vector of the system in the case of free vibration and λ is the modal frequency.

Substituting Equation (8) into Equation (7), we can get the following equation:

$$\left(\mathbf{K} - \lambda^2\mathbf{M}\right)\mathbf{A} = \mathbf{O}. \tag{9}$$

In order to obtain the generic natural frequencies of the dynamic system, the eigenvalues problem has to be solved by the following equation:

$$\mathrm{Det}\left(\mathbf{K} - \lambda^2\mathbf{M}\right) = 0. \tag{10}$$

The above equation is the algebraic equation of the 6 power real coefficient of λ^2, and the natural frequencies of the system can be obtained by solving it. The vibration mode of the structure can be obtained by substituting λ into Equation (9).

In this paper, we use a large linear vibrating screen with the size of 2500 mm × 6000 mm as a research object. The kinetic parameters are shown in Table 1.

The calculated natural frequency and corresponding system vibration are shown in Table 2.

The first six vibration modes of the system are presented graphically in Figures 3 and 4. They are rigid modal, and the modal frequency is lower which depends on the vibration mass and stiffness of spring. With the aim to simplify the analysis, both translational vibration modes and rotational vibration modes are plotted, respectively. In Figures 3 and 4, it can be seen that the fourth-order vibration mode (3.73 Hz) is mainly represented by translation in x direction. The other modes are obtained by the coupling effect of translation and rotation, which is mainly because of unsymmetrical installation position of spring from the center of mass on the x-y plane, and there is an offset between the spring mounting plane and the center of mass in the z plane, which leads to the existence of a nondiagonal element in the stiffness matrix; therefore, the translational and rotational motions are not completely decoupled.

3. Analysis of Finite Element Model Structure

To verify the results obtained by theoretical analysis and to optimize the structure dynamics, the finite element model of vibrating screen was set up using the finite element software ANSYS (Figure 5). The vibration exciters were replaced by the concentrated mass points with the same quality because the elasticity of vibrating vibrator was very small. The material properties defined the elastic modulus as $E = 2.030 \times 10^{11}$ Pa, and Poisson ratio was $u = 0.3$. The modal analysis was performed for the vibrating screen structure, and the first ten order modes were obtained. However, only the first six order rigid body modal shapes were compared (Figure 6).

The comparison of results obtained by theoretical analysis and finite element analysis for the first six order modes is shown in Table 3, wherein it can be seen that the value of natural frequency obtained by finite element analysis is in good agreement with the value obtained by theoretical calculation, and the maximal relative error is 5.69%.

In particular, the error of the torsional mode (3rd, 5th, and 6th orders) is greater than that of the translational mode (1st, 2nd, and 4th orders), which is due to the linearization simplification of torsion in the theoretical model. The motion trend of the sieve, as shown in Figure 6, is the same as that shown in Figures 3 and 4. Therefore, it is shown that the boundary conditions of the finite element model are consistent with the theoretical model. The finite element model can reflect the dynamic characteristics of the system, which can be used as a basis for further dynamic analysis and structural optimization.

4. Structural Optimization Analysis

4.1. Establishment and Fitting of BP Neural Network Model. For analysis of the elastic deformation of the vibration screen in the movement process, the 7th, 8th, 9th, and 10th order

Table 1: The kinetic parameters of the ZS2560 vibrating screen.

Parameter	Numerical value
m	7290 kg
J_{xx}	11875 kg·m^2
J_{yy}	19632 kg·m^2
J_{zz}	27233 kg·m^2
k_x, k_y, k_z	1.2×10^6 N/m,4×10^6 N/m, 1.2×10^6 N/m
l_{xy}	−0.543 m
l_{zx}, l_{yx}	2.52 m rear front 2.33 m rear back
l_{xz}, l_{yz}	1.54 m

Table 2: Modal calculation results of the vibrating screen (1~6 order).

Order	Natural frequency (Hz)	Natural modes of vibration
1	1.9947	$[0, 0, 1, 0.0834, 0.0157, 0]^T$
2	2.0346	$[-1, -0.002, 0, 0, 0, 0.0151]^T$
3	3.5803	$[0, 0, 0.0383, 0.0262, -1, 0]^T$
4	3.7300	$[0, 1, 0, 0, 0.0, 0]^T$
5	4.6042	$[0, 0, -0.1491, 1, 0.0152, 0]^T$
6	6.6498	$[0.0566, 0.0429, 0, 0, 0, 1]^T$

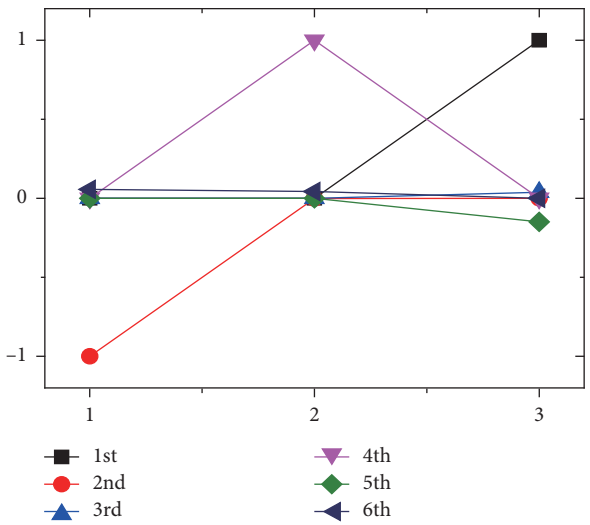

Figure 3: Translational vibration mode of 1–6 orders. 1: x direction degree of freedom; 2: y direction degree of freedom; 3: z direction degree of freedom.

modes were extracted, which are deformable modes, and modal frequency lies on structural stiffness of the vibrating screen. In Figure 7 and Table 4, there are two elastic modals around the working frequency (16 Hz), that are the ninth modal (14.697 Hz) and the tenth modal (21.968 Hz), which take a central part to the total deformation of the vibrating screen and are easy to lead to resonance. We can see that the main elastic deformation takes place at the side plate, which has low torsional stiffness and bending stiffness. In addition, the bending stiffness of the lower part is related to the screen frame tailgate, and torsional stiffness of the lower part is related to the sieve frame at the front outlet. The main

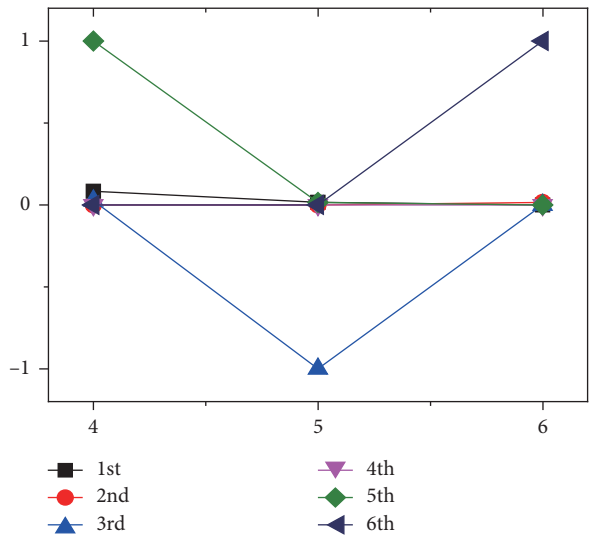

Figure 4: Torsional vibration mode of 1–6 orders. 4: ψ_x direction degree of freedom; 5: ψ_y direction degree of freedom; 6: ψ_z direction degree of freedom.

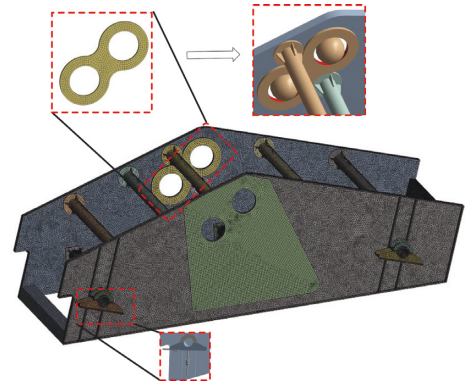

Figure 5: Grid partition of vibrating screen and boundary condition setting.

deformation occurs on the lateral plate, so it is necessary to optimize the strength by adjusting the beam position in order to improve lateral stiffness.

On the basis of modal analysis, the harmonic response analysis was carried out based on the modal superposition method, and the exciting force $F = 150000$ N was applied to the installation position of the exciter, while the working frequency was 16 Hz.

The relationship between structure design variables of vibration system and its dynamic characteristics is highly nonlinear. For complex systems, the relation between these parameters and performance cannot be expressed explicitly by a linear function, and direct optimization of these parameters is costly to calculate. However, the artificial neural networks (ANNs) have a very strong nonlinear mapping ability [24], so ANNs are very suitable for establishing the model of the vibration system. Currently, the BP neural network is the most widely used neural network model. Moreover, it has been proven theoretically that a three-layer BP network can approximate any rational function [25, 26].

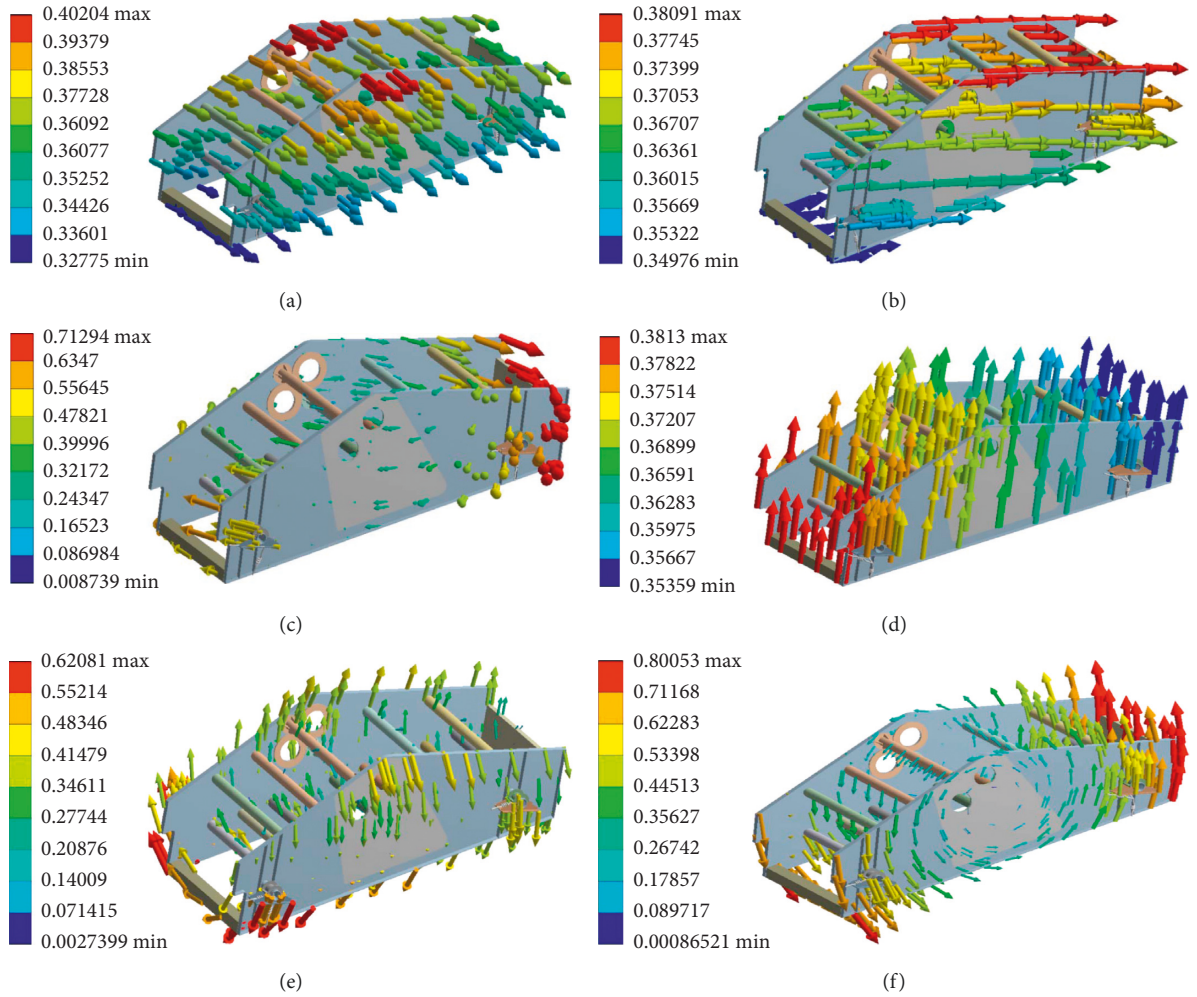

Figure 6: Modal picture of vibrating screen (1~6 orders). (a) 1st order. (b) 2nd order. (c) 3rd order (d) 4th order. (e) 5th order (f) 6th order.

Table 3: Comparison of FEM results with theoretical values.

Order	1	2	3	4	5	6
FEM results (Hz)	1.9774	2.0166	3.6141	3.7023	4. 8486	6.2717
Theoretical values (Hz)	1.9947	2.0346	3.5803	3.7300	4.6042	6.6498
Error (%)	−0.87	−0.88	0.94	−0.74	5.31	−5.69

Therefore, the BP neural network shown in Figure 8 is used to model the relationship between elastic deformation of vibrating screen and its design variables.

The sigmoidal function (*sigmoid*) was selected as an activation function of the hidden layer in BP ANN, and the linear function (*pureline*) was used as a transfer function of the output layer. Therefore, the entire network transfer function can be expressed as

$$G(X) = b_{2k} + \sum_{i=1}^{N_I} v\left(b_{1i} + \sum_{j=1}^{N_I} \eta_{ij} x_j\right), \tag{11}$$

where η_{ij} is the network connection weight value; b_{1i} and b_{2k} are threshold values for network connections; v is the implicit excitation function; N_I is the number of input layer nodes, $N_I = 12$; and N_J is the number of hidden layer nodes, which is calculated according to the formula

$$N_J \le \sqrt{N_J + q} + s, \tag{12}$$

where q is the number of output elements, $q = 1$, and s is the constant between 0 and 10, $s = 2$.

The input parameters of the network are the horizontal and vertical installation position of beams which is shown in Figure 9, while the output parameter is the maxelastic deformation of the screen box of ZS2560.

Design of the neural network model requires ANNs training with a certain number of samples with a proper distribution to make the neural network learn and express the relation accurately. In order to meet the requirements of

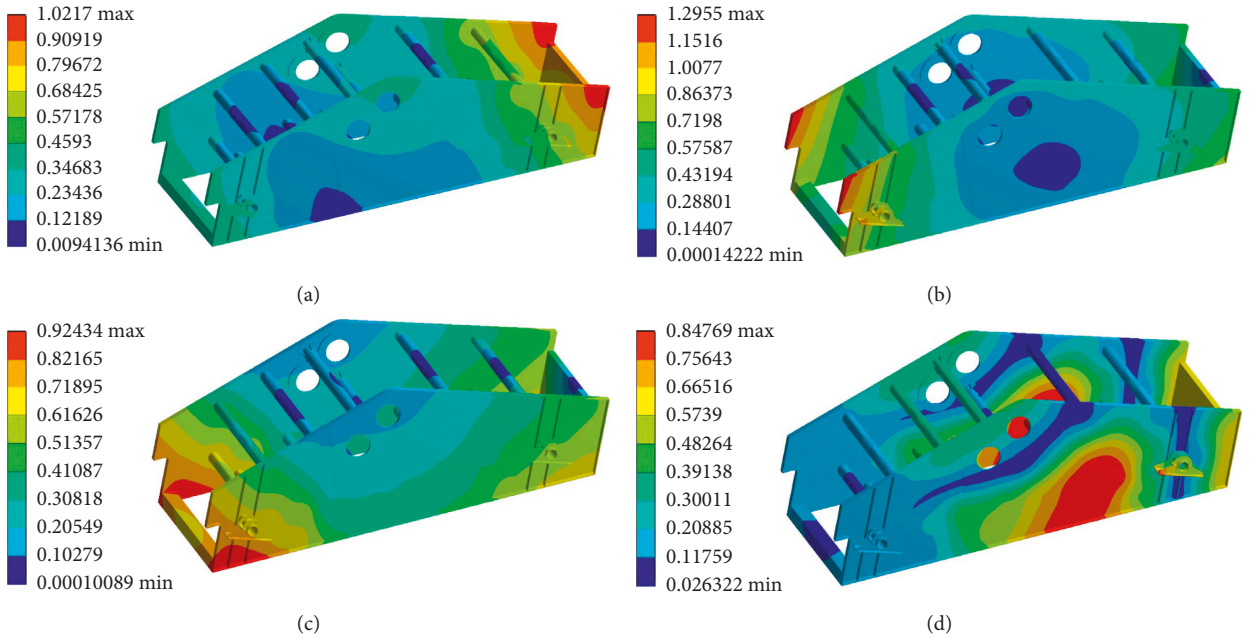

Figure 7: Modal picture of vibrating screen (7~10 order). (a) 7 order. (b) 8 order. (c) 9 order. (d) 10 order.

Table 4: Modal calculation results of vibrating screen (7~10 order).

Order	Natural frequency f (Hz)
7	11.028
8	13.372
9	14.697
10	21.968

both test workload and design accuracy, the orthogonal test design method is used to select a few representative schemes from a large number of test schemes.

In design optimization, first the design variables were defined, and then positions of 6 strengthening beams in x and y dimensions were labeled as a–f and set as design parameters, as shown in Figure 9.

Through the orthogonal design with 12 factors and 3 levels, 27 sets of parameter combinations were obtained. The finite element model was established, and the corresponding elastic deformation was calculated.

In order to more intuitively reveal the trend of the test results changing with the level of each factor, the range analysis method was used to analyze the results of the orthogonal test directly. The trend of the 12 factors in this experiment is shown in Figure 10. For each factor, the abscissa is the horizontal number and the ordinate is the corresponding mean. According to Figure 10, for factors a_x and b_y, as the value increases, the elastic deformation of the structure increases. For the factors a_y, b_x, c_x, and c_y, as the value increases, the elastic deformation of the structure increases first and then decreases. Besides, for other factors, as the value increases, the elastic deformation of the structure decreases. In particular, for the factor d_x, as the value increase, the elastic deformation of the structure keeps 5.644 mm, which means the effect of the variable on the elastic deformation in the first interval is weak.

On the basis of the orthogonal test, the qualitative law of structural deformation was obtained through the range analysis method. In order to more accurately design the structure, neural network modeling and parameter optimization are required. According to the structure shown in Figure 8, a neural network model with 12 inputs and 1 output was constructed. Twenty-seven groups of orthogonal test data were divided into training group and test group, in which the training group contains 20 groups of data and the test group contains 7 groups of data. The Levenberg–Marquardt algorithm was used as the training function of the neural network to improve the convergence speed of the model. After the iterative training, the simulation results and error distribution were as shown in Figure 11, where the error between simulation results and training results is acceptable. After training, we tested the network with the samples which were not used for the training, and the agreement of ANN output and real output is presented in Figure 12, wherein it can be seen that the maximal error is less than 1.6%; thus, a high-degree agreement is achieved.

4.2. Genetic Algorithm Optimization. The GA simulates the Darwinian evolution genetic selection, i.e., the evolution process of survival of the fittest rules with the same group of chromosome, by a random search algorithm combining the information transformation mechanism, initialization parameter coding, and initial population, and then by using the crossover operation and mutation, natural selection operator, parallel iteration, and optimization solutions [27].

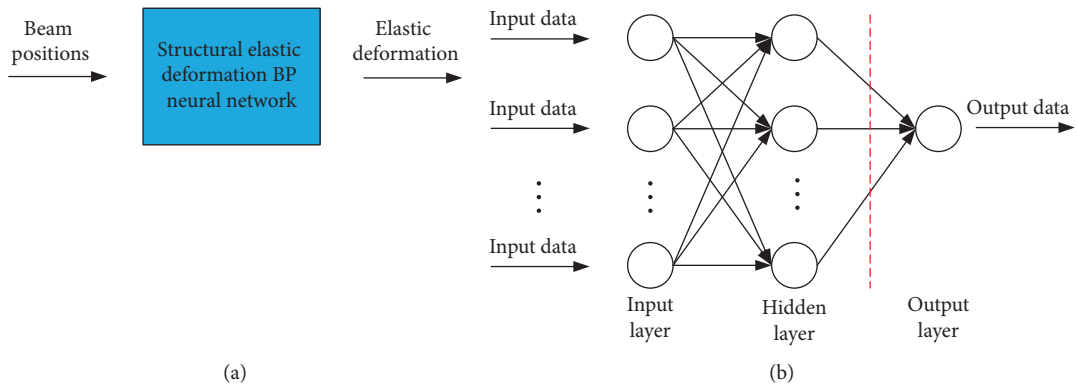

Figure 8: BP neural network prediction model for structural elastic deformation. (a) Input and output parameters of BP neural network model. (b) BP neural network model structure.

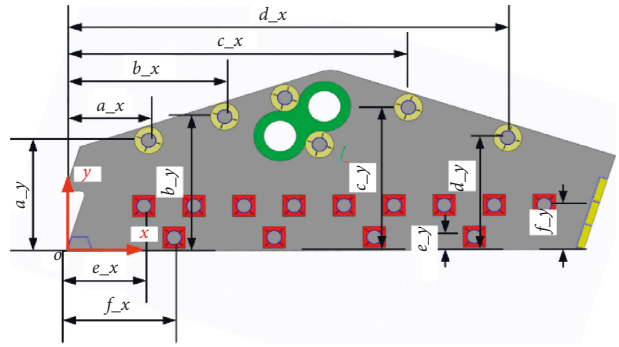

Figure 9: Schematic diagram of design variable for the vibrating screen.

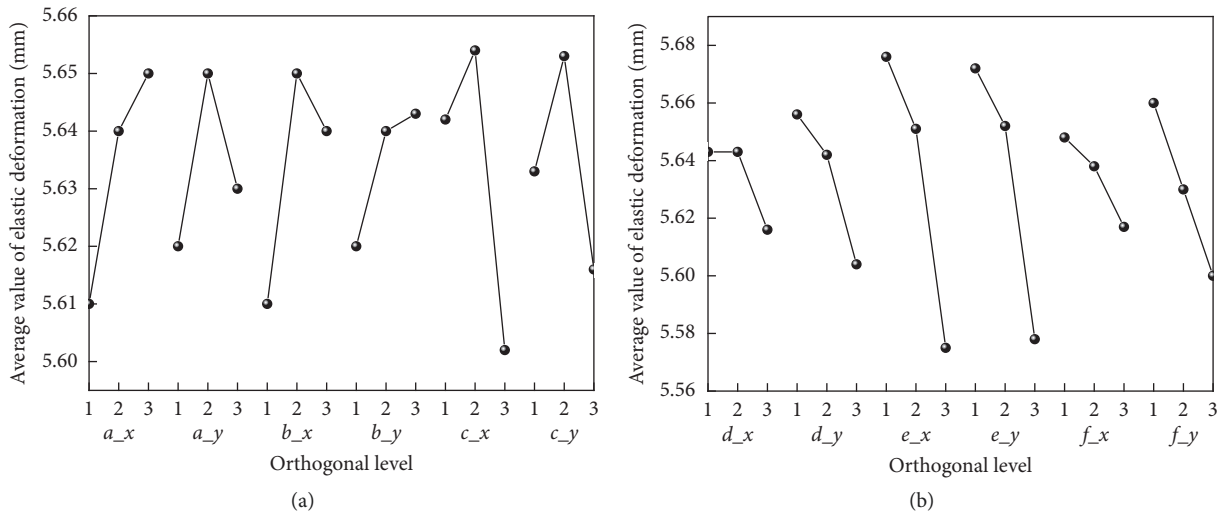

Figure 10: Trend diagram of relationship between beam positions and elastic deformation.

Since GA is based on random operation, there are no special requirements for search space, and derivation is not needed. Due to the advantages of simple operation and fast convergence speed, GA has quickly developed in recent years, and it has been widely used in combinatorial optimization, adaptive control, and many other engineering fields. Based on the research results in Section 4.1, the optimization flow chart of this paper is shown in Figure 13.

In order to reduce the elastic deformation by searching the optimal beams position, the genetic algorithm is selected to optimize the BP network model established, and it is defined by

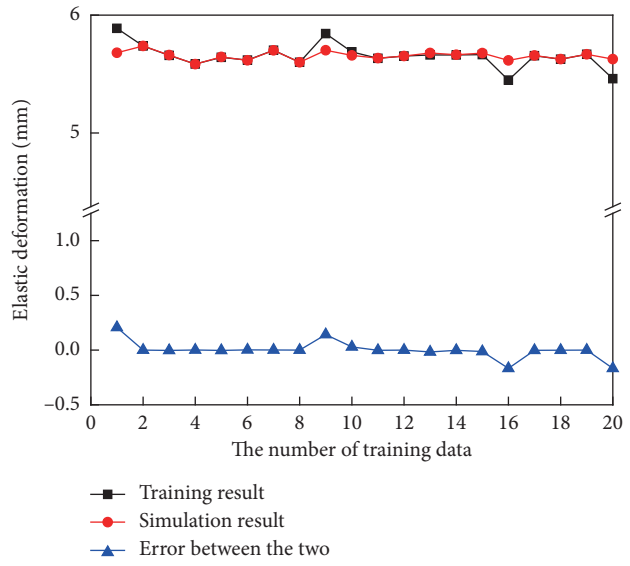

Figure 11: Comparison between the training results and the simulation results.

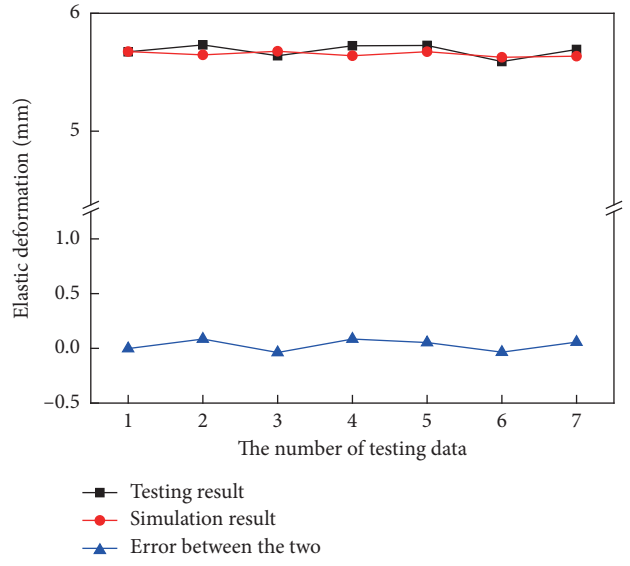

Figure 12: Comparison between the testing results and the simulation results.

$$\begin{cases} Find & X = \{x_1, x_2, \ldots\ldots x_{12}\}^T, \\ \min & G(X), \\ \text{s.t.} & x_i^L \le x_i \le x_i^U, \end{cases} \tag{13}$$

where $X = \{x_1, x_2, \ldots\ldots x_{12}\}^T$ is defined design variables; x_1~x_2 correspond to the position of a ~ f beam; $G(X)$ is the optimized target function; x_i^L and x_i^U are the upper and lower limits of the design variables. Considering the side plate shape and the sieving position, x_i^L and x_i^U are defined as shown in Table 5.

Sensitivity analysis can determine the gradient relationship between the design variable and the objective function and reflect the contribution of the design variable to the change of the objective function.

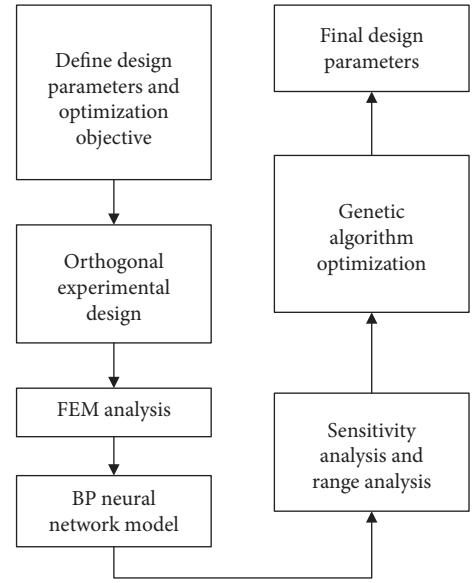

Figure 13: Optimization flow chart of the large vibrating screen.

The differential form sensitivity of the design variable is defined by the following equation:

$$\frac{\partial G}{\partial x_i} = \frac{G(\mathbf{X} - \Delta x_i \mathbf{e}) - G(\mathbf{X})}{\Delta x_i}, \tag{14}$$

where $\mathbf{e}$ is the array with the same number of $\mathbf{X}$ vectors, 1 at x_i and 0 at the rest, and Δx_i is the change in design variables.

Based on the BP neural network model established in Section 4.1, the differential form sensitivity of the design variable has been obtained by perturbing the design variable to calculate the change degree of the objective function. The final result is shown in Figure 14.

As shown in Figure 14, the elastic deformation is more sensitive to the x-coordinate of the beams than the y-coordinate. Therefore, this indicates that more attention should be paid to the horizontal coordinates of beams in the further optimization processes. Besides, except the beam a, the sensitivity of elastic deformation to the position of other beams is negative, which means that the increase of beam coordinates will lead to the decrease of elastic deformation. The sensitivity analysis results can be used as a criterion to evaluate the optimization results.

The genetic algorithm parameter settings are shown in Table 6, and the estimated and target values were calculated for the minimum of objective function in the feasible region shown in Table 5.

The iterative histories for objective function are shown in Figure 15. In the initial state, the results obtained by the genetic algorithm fluctuate greatly. After 20 generations, with the increase of the number of iterations, the results converge gradually. Finally, the optimization results tend to be stable.

The optimal design variables obtained by the genetic algorithm are compared with the original design variables in Table 7. The obtained design parameters are added to the finite element model, and the optimized results are obtained.

Table 5: The upper and lower bounds of design variables (mm).

i	1	2	3	4	5	6	7	8	9	10	11	12
x_i^L (mm)	800	1200	1722.4	1596	4020	1705	5107	1219	900	500	1100	120
x_i^U (mm)	1200	1600	2122.4	1996	4620	2005	5607	1619	1400	800	1500	240

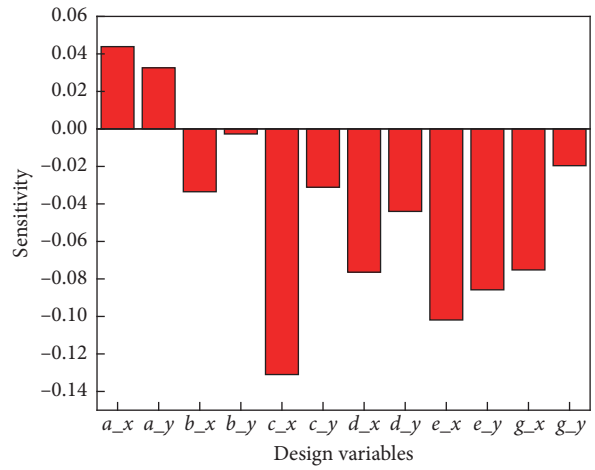

Figure 14: The sensitivity of design variables.

Table 6: The genetic algorithm parameter settings.

GA parameters	Explain
Coding method	Binary coding
Ordering method	Ranking compositor
Selection method	Roulette
Cross method	Random multipoint intersection
Variation method	Disperse multipoint variation
Population size	200
Crossover probability	0.8
Mutation probability	0.1
Evolutionary algebra	200

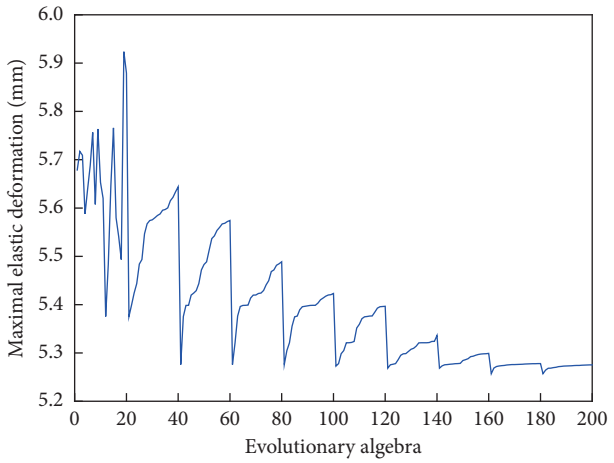

Figure 15: The iterative histories for objective function.

After optimization, the maximal elastic deformation was 5.283 mm, and compared to the initial value, it was reduced for 6.99%.

Table 7: Optimized design variables.

Parameters	Original value (mm)	Optimal value (mm)	Round (mm)
a_x	1126	814.4550945	814.5
a_y	1400	1274.839705	1275
b_x	1922.4	1751.020621	1751
b_y	1696	1688.835332	1689
c_x	4120	4587.176421	4587
c_y	1805	1924.636191	1925
d_x	5307	5571.593556	5572
d_y	1419	1432.600318	1433
e_x	939.6	1319.516474	1320
e_y	570	786.8099837	787
f_x	1300	1355.805261	1356
f_y	170	219.2089448	219
Maximal elastic deformation	5.68	—	5.283

From Table 7, it can be seen that the factors a_x and b_y are lower than the initial values after optimization and other factors are higher than the initial values. The variation law of each factor is consistent with the qualitative law obtained by the range analysis method. Therefore, the optimization results obtained by neural networks and genetic algorithms are credible.

5. Conclusion

A new structural solution for high loaded vibrating screens was proposed in this paper, and the following conclusions are obtained:

(1) The dynamic model of the vibrating screen with 6 degrees of freedom is established based on the Lagrange equation. By numerical calculation, the first six orders natural frequency and the corresponding vibration mode of rigid body as well as the distribution law of rigid body modes are obtained by numerical calculation. Among them, the 1st mode (1.9947 Hz), 2nd mode (2.0346 Hz), and 4th mode (3.5803 Hz) are mainly translational motion, and the 3rd mode (3.5803 Hz), 5th mode (4.6042 Hz), and 6th mode (6.6498 Hz) are mainly translational motion. By means of the vibration mode, the complex space motion of the vibrating screen is dynamically decoupled and the dynamic decoupling condition of the vibrating screen is given.

(2) The excitation frequency range that influences the steady state operation of the vibrating screen is analyzed, and the maximum error between the finite element model and the theoretical value is 5.69%, the feasibility and accuracy of the finite element model in describing the vibration characteristics of the system are verified.

(3) Based on the orthogonal test and finite element analysis, the BP neural network is used to model the relationship between design variables and elastic deformation of the vibrating screen. And the sensitivity of each variable to structural elastic deformation is analyzed; the elastic deformation is more sensitive to the x-coordinate of the beams than the y-coordinate.

(4) Genetic algorithm is used for optimization. According to the obtained results, the maximum elastic deformation was reduced by 6.99% compared to the original design.

This optimization design is simple and flexible; it shortens the design period and applies to other similar products.

Nomenclature

$\mathbf{A}$: The amplitude vector of the system in the case of free vibration
b_{1i}, b_{2k}: Threshold values for network connections
$\mathbf{F}$: The excitation matrix of the system
J_{xx}: The moments of inertia of the vibrating screen with respect to x-axis (kg·m^2)
J_{yy}: The moments of inertia of the vibrating screen with respect to y-axis (kg·m^2)
J_{zz}: The moments of inertia of the vibrating screen with respect to z-axis (kg·m^2)
J_{xy}: The product of inertia in the x-y plane (kg·m^2)
J_{yz}: The product of inertia in the y-z plane (kg·m^2)
J_{xz}: The product of inertia in the x-z plane (kg·m^2)
k_x: The stiffness of springs in the x direction (N/m)
k_y: The stiffness of springs in the y direction (N/m)
k_z: The stiffness of springs in the z direction (N/m)
l_{ij}: The spatial position of the spring (m)
m: The mass of the vibrating screen (kg)
m_0e: The product of eccentric mass diameter of the exciter (kg·m)
N_I: The number of input layer nodes
N_J: The number of hidden layer nodes
q: The number of output elements
x, y, z: The translational degrees of freedom in the x, y, and z directions (m)
ψ_x, ψ_y, ψ_z: The rotation degrees of freedom in the x, y, and z directions (rad)
ω: The rotation speed (rad/s)
α: The vibrating direction angle (rad)
δ: The normal distance between the center of mass and the excitation force direction (m)
λ: The modal frequency (Hz)
η_{ij}: The network connection weight value
υ: The implicit excitation function.

Data Availability

The data used to support the findings of this study are available from the corresponding author upon request.

Conflicts of Interest

The authors declare that there are no conflicts of interest regarding the publication of this paper.

Acknowledgments

This work has been supported in part by the National Natural Science Foundation of China (Project nos. 51775544 and U1508210).

References

[1] O. A. Makinde, B. I. Ramatsetse, and K. Mpofu, "Review of vibrating screen development trends: linking the past and the future in mining machinery industries," *International Journal of Mineral Processing*, vol. 145, pp. 17–22, 2015.

[2] S. Huband, D. Tuppurainen, L. While, L. Barone, P. Hingston, and R. Bearman, "Maximising overall value in plant design," *Minerals Engineering*, vol. 19, no. 15, pp. 1470–1478, 2006.

[3] S. Baragetti and F. Villa, "A dynamic optimization theoretical method for heavy loaded vibrating screens," *Nonlinear Dynamics*, vol. 78, no. 1, pp. 609–627, 2014.

[4] Y. Y. Wang, J. B. Shi, F. F. Zhang et al., "Optimization of vibrating parameters for large linear vibrating screen," *Advanced Materials Research*, vol. 490, pp. 2804–2808, 2012.

[5] Z. F. Li, X. Tong, B. Zhou, and X. Wang, "Modeling and parameter optimization for the design of vibrating screens," *Minerals Engineering*, vol. 83, pp. 149–155, 2015.

[6] X. M. He and C. S. Liu, "Dynamics and screening characteristics of a vibrating screen with variable elliptical trace," *International Journal of Mining Science and Technology*, vol. 19, no. 4, pp. 508–513, 2009.

[7] B. Zhang, J. K. Gong, W. H. Yuan, J. Fu, and Y. Huang, "Intelligent prediction of sieving efficiency in vibrating screens," *Shock and Vibration*, vol. 2016, Article ID 9175417, 7 pages, 2016.

[8] Y. M. Zhao, C. S. Liu, X. M. He, Z. Cheng-yong, W. Yi-bin, and R. Zi-ting, "Dynamic design theory and application of large vibrating screen," *Procedia Earth & Planetary Science*, vol. 1, no. 1, pp. 776–784, 2009.

[9] R. H. Su, L. Q. Zhu, and C. Y. Peng, "CAE applied to dynamic optimal design for large-scale vibrating screen," in *Proceedings of Acis International Symposium on Cryptography*, pp. 316–320, Heibei, China, 2011.

[10] S. Baragetti, "Innovative structural solution for heavy loaded vibrating screens," *Minerals Engineering*, vol. 84, pp. 15–26, 2015.

[11] L.-p. Peng, C.-s. Liu, B.-c. Song, J.-d. Wu, and S. Wang, "Improvement for design of beam structures in large vibrating screen considering bending and random vibration," *Journal of Central South University*, vol. 22, no. 9, pp. 3380–3388, 2015.

[12] Z. Q. Wang, C. S. Liu, J. Wu, H. Jiang, B. Song, and Y. Zhao, "A novel high-strength large vibrating screen with duplex statically indeterminate mesh beam structure," *Journal of Vibroengineering*, vol. 19, no. 8, pp. 5719–5734, 2017.

[13] H. Jiang, Y. Zhao, C. Duan et al., "Dynamic characteristics of an equal-thickness screen with a variable amplitude and screening analysis," *Powder Technology*, vol. 311, pp. 239–246, 2017.

[14] C. L. Du, K. D. Gao, J. Li, and H. Jiang, "Dynamics behavior research on variable linear vibration screen with flexible screen face," *Advances in Mechanical Engineering*, vol. 6, pp. 1–12, 2014.

[15] M. K. Rad, M. Torabizadeh, and A. Noshadi, "Artificial Neural Network-based fault diagnostics of an electric motor using vibration monitoring," in *Proceedings of 2011 International Conference on Transportation, Mechanical, and Electrical Engineering (TMEE)*, pp. 1512–1516, IEEE, Changchun, China, 2011.

[16] Z. G. Tian, "An artificial neural network method for remaining useful life prediction of equipment subject to condition monitoring," *Journal of Intelligent Manufacturing*, vol. 23, no. 2, pp. 227–237, 2012.

[17] V. Meruane and J. Mahu, "Real-time structural damage assessment using artificial neural networks and antiresonant frequencies," *Shock and Vibration*, vol. 2014, Article ID 653279, 14 pages, 2014.

[18] Y. Sun and J. Y. Han, "Monitoring method for UAV image of greenhouse and plastic-mulched Landcover based on deep learning," *Journal of Agricultural Machinery and Machinery (in Chinese)*, vol. 49, pp. 133–140, 2018.

[19] S. Zhang, Y. M. Liang, and J. Y. Wang, "Application of BP-ANN in optical coherent tomography images classification," *Journal of Optoelectronics Laser*, vol. 23, pp. 391–395, 2012.

[20] C.-s. Liu, S.-m. Zhang, H.-p. Zhou et al., "Dynamic analysis and simulation of four-axis forced synchronizing banana vibrating screen of variable linear trajectory," *Journal of Central South university*, vol. 19, no. 6, pp. 1530–1536, 2012.

[21] Y. Y. Li, C. X. He, X. D. Song et al., "Study on dynamic analysis and parameter influence of vibrating screen system of asphalt mixing equipment," *Chinese Journal of Computational Mechanics (in Chinese)*, vol. 32, pp. 565–570, 2015.

[22] W. Y. Li, C. Y. Mi, W. G. Wu et al., "Application of experimental modal analysis technique to structural design of linear vibrating screen," *Journal of Coal Science & Engineering (in Chinese)*, vol. 1, pp. 88–90, 2004.

[23] Y. Hou, L. Y. Wang, and J. Ma, "Free vibration analysis of shale shaker laminated flat-screen," *Journal of Mechanical Engineering*, vol. 51, no. 23, pp. 60–65, 2015.

[24] S. Umehara, T. Yamazaki, and Y. Sugai, "A precipitation estimation system based on support vector machine and neural network," *Electronics and Communications in Japan (Part III: Fundamental Electronic Science)*, vol. 89, no. 3, pp. 38–47, 2006.

[25] M. Y. Rafiq, G. Bugmann, and D. J. Easterbrook, "Neural network design for engineering applications," *Computers & Structures*, vol. 79, no. 17, pp. 1541–1552, 2001.

[26] M. T. Hagan, M. Beale, and M. Beale, *Neural Network Design*, China Machine Press, Beijing, China, 2002.

[27] A. Brabazon, O. M. Neill, and S. McGarraghy, *Genetic Algorithm*, Springer, Berlin, Germany, 2015.